Indian Journal of Chemistry
Vol. 60A, April 2021, pp. 531-537

Synthesis and crystal structures of 2-acetylpyridine-N(4)-methyl-3-thiosemicarbazone (L) and its metal complexes: Anticancer activity of [Cu(L)(OAc)]

Chinmoy Biswas[a], Arnab Chatterjee[a], Sreelekshmi Sreekumar[b], Manikantan Syamala Kiran[b,]* & Rajarshi Ghosh[a,]*

[a]Department of Chemistry, The University of Burdwan, Burdwan 713 104, India

[b]Biological Materials Laboratory, CSIR-Central Leather Research Institute, Chennai 600 020, India

*E-mail: kiran@clri.res.in (MSK)/ rghosh@chem.buruniv.ac.in (RG)

Received 23 November 2020; revised and accepted 23 February 2021

Synthesis and structural characterization of N(4)-substituted 2-acetylpyridine-N(4)-methyl-3-thiosemicarbazone (**L**) and its two metal complexes [Cu(L)(OAc)] (**1**) and $[ZnL(OAc)]_2$ (**2**) are reported. Between the two complexes **1** is found to have good anticancer activity against Human lung cancer cell line (A549). Fluorescence microscopy finds the formation of reactive oxygen species on treatment of the cancer cells with **1**. The IC_{50} value of the complex is measured as 0.72 µM which is lower than that of cisplatin against A549.

Keywords: Cu(II), Zn(II), Thiosemicarbazone, X-ray structure, Anticancer activity

Thiosemicarbazones are an important class of (N, S) donor ligands having its thione and thiolate tautomeric forms, and showing a number of biological activities[1,2]. Several coordination modes of these ligands towards metal centres have made them interesting[3] in designing metal based cancer chemotherapeutic drugs. Cisplatin and related platinum drugs fascinated the coordination chemists during last few decades[4] as an alternative to cancer treatments. But the limitation of these compounds towards successful cancer chemotherapy is due to their DNA mismatch repair. For this very reason different first row transition metal-based drugs are now being synthesized[3-5] as an alternative to cisplatin and its derivatives. The additional advantage in this type of drugs is that the most of the transition metals used are essential trace elements in human physiological systems. In case of thiosemicarbazones, the ligand backbone often plays an important role in exhibiting biological activities. Moreover, the biological activities of metal thiosemicarbazones are highly dependent on various substitutions on the ligand framework. According to previous reports[6,7], substitution on terminal nitrogen [N(4)] of the thiosemicarbazones makes significant changes in their activities. In continuation to our earlier interests in designing transition metal based cancer chemotherapeutic agents[8], here we have designed and synthesized a N(4)-substituted 2-acetylpyridine-N(4)-methyl-3-thiosemicarbazone (**L**) (Scheme 1) and their two transition metal complexes CuL(OAc) (**1**) and $[ZnL(OAc)]_2$ (**2**). The ligand and each of the metal complexes are characterized X-ray crystallographically. Crystal structure of **L** was previously reported[9]. The complexes along with the ligand here reported are used in investigating the anticancer activity against human lung cancer cell line. Except the complex **1**, other compounds were found similarly toxic to normal healthy cells. So, the detailed investigation regarding cell viability, reactive oxygen species (ROS) generation, etc. are performed using the complex **1** only.

Materials and Methods

Materials

2-acetylpyridine (Sigma-Aldrich, UK), 4-methyl-3-thiosemicarbazide (Sigma-Aldrich, UK), zinc(II) acetate dihydrate (SRL, India), copper(II) acetate dihydrate (SRL, India) were purchased and used as received. Solvents were dried using standard procedure and distilled before use.

Physical measurements

Elemental analyses (carbon, hydrogen and nitrogen) were performed on a PerkinElmer 2400 CHNS/O

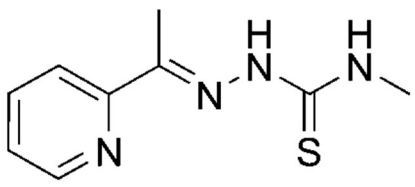

Scheme 1 — Molecular structure of 2-acetylpyridine-N(4)-methyl-3-thiosemicarbazone (**L**)

elemental analyzer. UV-visible absorption, IR (KBr discs, 4000-500 cm^{-1}) and ^{1}H-NMR spectra were recorded using a Shimadzu UV-Vis 2450 spectrophotometer, PerkinElmer FT-IR model RX1 spectrometer and Bruker Advance III 500 MHz (and 400 MHz) NMR spectrometer, respectively.

X-ray diffraction

Single crystals of **L**, **1** and **2** suitable for X-ray crystallographic analysis were selected following examination under a microscope. Diffraction data at 293 K (for **L**) and 296 K (for **1** and **2**) were collected on Bruker-Kappa APEX II CCD diffractometer using Cu-Kα (λ = 1.54184 Å) and Mo-Kα radiations (λ = 0.71073 Å), respectively. The data collection parameters and crystal data are listed in Table 1. The compounds **L** and **1** were crystallized in $P2_1/c$, and **2** were in $P2_1/n$, respectively. Of 8159 (**L**), 26816 (**1**) and 23481(**2**) collected reflections, respective 2050, 3404 and 2966 unique reflections with I>2σ(I) were used for structure solution. The structures were solved by direct methods and the structure solution and refinement were based on $|F|^2$. The final differences Fourier map showed the maximum and minimum peak heights at 0.405 and -0.303 eÅ^{-3} for **L**, 0.616 and -0.404 eÅ^{-3} for **1**, 0.704 and -0.514 eÅ^{-3} for **2** with no chemical significance. All calculations were carried out using SHELXL-97[10] and ORTEP-32[11].

Synthesis of ligand and its metal complexes

Synthesis of N(4)-substituted 2-acetylpyridine-N(4)-methyl-3-thiosemicarbazone L

The ligand **L** was synthesized by a modified reported method[9]. Ethanolic solution (50 mL) of 2-acetylpyridine (230.77 mg, 1.905 mmol) and 4-methyl-3-thiosemicarbazide (200.00 mg, 1.905 mmol) were mixed in a 100 mL round bottom flask. The reaction mixture was refluxed for 10 h. On evaporation of the final ethanolic mixture on steam bath off white block shaped crystals appeared. It was dried *in vacuo* and dissolved in ethanol for recrystallization. Single crystals of **L** were appeared after a week.

Yield: 0.278 g (70%), Anal. for $C_9H_{12}N_4S$ (**L**): Calcd. (%) C, 51.89; H, 05.80; N, 26.89; found (%), C, 51.77; H, 05.75; N, 26.99; Selected IR bands (KBr pellet, cm^{-1}):1606.00 ($\nu_{C=N}$), 778.99 (ν_{C-S}); UV-visible absorption (λ, nm): 320; ^{1}H NMR ($CDCl_3$, 500 MHz): δ_H (ppm) = 2.35 (s, 3H), 3.22 (d, 3H. J = 6Hz), 7.63 (m, 1H), 7.64-8.68 (m, 4H).

Synthesis of CuL(OAc) (1)

Copper(II) acetate dihydrate (19.96 mg, 0.1 mmol) was slowly added to the ethanolic solution of **L** (20.81 mg, 0.1 mmol) and the reaction mixture was stirred for about 3 h. The resulting solution turned light yellow and then it was filtered. Finally, the mixture was kept on slow evaporation. This yielded dark brown coloured X-ray quality single crystals of the complex within a week. These were separated by filtration, washed and finally dried *in vaccuo*.

Yield: 0.002 g (68%), Anal. for $C_{11}H_{16}N_4O_3SCu$ (**1**): Calcd. (%), C, 46.46; H, 05.67, N, 19.70; found (%), C, 46.41; H, 05.59; N, 19.75; Selected IR bands (KBr pellet, cm^{-1}): 1586.20 ($\nu_{C=N}$), 776.78 (ν_{C-S}); UV-visible absorption (λ, nm): 323, 405.

Synthesis of [ZnL(OAc)]$_2$(2)

Ethanolic solutions of each of the **L** (20.80 mg, 0.1 mmol) and zinc(II) acetate dihydrate (24.14 mg, 0.1 mmol) were mixed and stirred for an hour. On stirring there was no appreciable colour change of the final solution which was filtered and kept on air for slow evaporation. After a week or so, intense yellow coloured single crystals were appeared. These were separated by filtration, washed and finally dried *in vaccuo*.

Yield: 0.004 g (68%), Anal. for $C_{22}H_{28}N_8O_4S_2Zn_2$ (**2**): Calcd. (%), C, 49.60; H, 5.29; N, 21.03; found (%), C, 49.56; H, 5.26; N, 21.11; Selected IR bands (KBr pellet, cm^{-1}): 1582.00 ($\nu_{C=N}$), 752.72 (ν_{C-S}); UV-visible absorption (λ, nm): 324; ^{1}H NMR ($CDCl_3$, 400 MHz): δ_H (ppm) = 2.53 (s, 3H), 7.64-8.79 (m, 4H), 1.98 (s, 6H), 3.10 (s, 3H)

Anticancer activity

Cell viability assay

The cell viability of samples (**L**, **1** and **2**) were analysed by MTT [3-(4, 5-dimethylthiazol-2-yl)-2,5-diphenyl tetrazolium bromide] assay. Immortalized Human lung epithelial cell lines (L132) and Human lung cancer cell lines (A549) were used. Approximately 12,000 cells were seeded into 48 well culture plates and were incubated in CO_2 incubator for 24 h. Both cells were then treated with different concentrations [10 ng/mL, 25 ng/mL, 50 ng/mL, 100 ng/mL, 250 ng/mL, 500 ng/mL, 1000 ng/mL] of all the five samples. After 24 h of incubation, the treatment medium was removed and the cells were treated with 0.5 mg/mL MTT salt. After 4 h of incubation, the purple coloured formazan crystals were solubilized in dimethyl sulfoxide and absorbance was read at 570 nm in Bio-Rad Elisa plate reader. The cell viability was calculated by the following formula

$$\%\ \text{of cell viability} = \frac{\text{OD of treated culture}}{\text{OD of control}} \times 100$$

Reactive oxygen species (ROS) generation

To determine the ROS generation, cells were treated with different concentrations of the sample. After 24 h of incubation, the cells were washed with phosphate-buffered saline and incubated with 5 μM 2′,7′-dichlorofluorescin diacetate (DCFH-DA) in PBS for 30 min. After incubation, images of the cells were captured at 495 nm excitation and 523 nm emission (blue filter) using Leica DMi8 fluorescent microscope, Leica micro systems, Germany.

Results and Discussion

Synthesis and formulation

Equimolecular mixture of 2-acetylpyridine and 4-methyl-3-thiosemicarbazide were refluxed for 10 h to get the ligand **L**, which was characterized spectroscopically as well as X-ray crystallographically. In IR spectra, bands at 1606 and 779 cm^{-1} refers to respective imine and thione functions of the ligand[12]. In complexes, because of donation of electron density from the N- and S- donor centre the C=N (in imine) and C-S stretchings are expectedly decreased. In ^1H NMR analysis (Supplementary Data, Fig. S1), a singlet peak is observed at 2.35 ppm is due to three methyl protons attached to the imine group. The terminal methyl protons attached with the secondary amine group are to some extent deshielded and the doublet signal at 3.22 ppm may be assigned for those. The terminal secondary amine proton which is very much deshielded expectedly appears at very much downfield (7.63 ppm) as multiplet. The four aromatic protons attached with the pyridine moiety appear at 7.64-8.68 ppm as multiplet. For measuring the absorption spectra, ethanol is used as the solvent as **L** and its metal complexes (**1** and **2**) are soluble in ethanol. In absorption spectra, a band at 320 nm appears, which may be because of n-π*/π-π* transition. In absorption studies, the complex (**1**) showed band in visible region.

X-ray structures of L, 1 and 2

Single crystal X-ray diffraction of the ligand **L** and the metal complexes (**1** and **2**) were done. The crystallographic parameters are listed in Table 1.

Table 1 — Crystallographic parameters of **L**, **1** and **2**

Parameters	**L**	**1**	**2**
Formula	$C_9H_{12}N_4S$	$C_{11}H_{16}N_4SO_3Cu$	$C_{22}H_{30}N_8O_4S_2Zn_2$
Mol. wt.	208.28	347.88	665.40
Crystal system	monoclinic	Monoclinic	monoclinic
Space group	P 21/c	P 21/c	P 21/n
Temperature (K)	293	296	296
Wavelength	1.54184	0.71073	0.71073
a (Å)	8.8119(3)	7.03040(10)	10.5447(2)
b (Å)	7.7228(2)	11.1579(2)	8.2796(2)
c (Å)	15.5830(5)	19.4098(4)	16.1813(4)
α (°)	90	90	90
β (°)	106.125(3)	99.4140(10)	99.949(1)
γ (°)	90	90	90
V ($Å^3$)	1018.74(6)	1502.09(5)	1391.48(6)
Z	4	4	2
D_c (g cm^{-3})	1.358	2.393	1.588
M (mm^{-1})	2.544	5.414	1.918
F(000)	440.0	1050.0	684.0
R(int)	0.044	0.0206	0.021
Total reflections	8159	26816	23481
$I > 2\sigma(I)$	2050	3404	2966
Completeness to theta	0.976	0.996	0.997
Absorption correction	multi-scan	multi-scan	multi-scan
θ_{max} and θ_{min}	79.23° and 5.24°	28.315° and 2.127°	28.30° and 2.15°
Data/restraints/parameters	2149/0/130	3724/ 0/ 193	3445/0/176
Goodness-of-fit (GOF) on F^2	1.067	1.147	1.094
Final R indices [l > 2s(l)]	R1 = 0.0461 and wR2 = 0.1254	R1 = 0.0293 and wR2 = 0.0833	R1=0.0296 and wR2=0.0765
R indices (all data)	R1 = 0.0478 and wR2 = 0.1266	R1 = 0.0342 and wR2 = 0.0933	R1 = 0.0380 and wR2 = 0.0802
Largest difference in peak and hole (e$Å^{-3}$)	0.405, -0.303	0.616, -0.404	0.704, -0.514

2-acetylpyridine-N(4)-methyl-3-thiosemicarbazone (L)

Thermal ellipsoid plot of **L** is given in Fig. 1a. Bond angles and bond distances of different bonds as calculated from the single crystal data are shown in Table 2. For **L**, the C-S bond distance is found to be 1.6874(15) Å which is suggestive of the thione form[9].

CuL(OAc) (1)

ORTEP representation of **1** is given in Fig. 1b. From Table 2, the bond distance and bond angles indicate a distorted square planar structure for the tetracoordinated Cu(II) centre in complex **1**. The pyridine nitrogen (N(008)) and the thiolsulfur (S(002)), and the imine nitrogen (N(005)) and acetate oxygen (O(1)) are in *trans* position of the distorted square planar geometry. The difference between the maximum and minimum bond distances in the distorted square plane is 0.2779 Å. The C-S bond distance in the ligand backbone of **1** is 1.7503 Å. This larger bond distance (2.23 Å) is suggestive of the thiolate form of the C-S bond of the **L** as well as +II oxidation level of the metal in the complex (as one acetate is coordinated with the metal)[13].

[ZnL(OAc)]$_2$ (2)

The molecular structure of **2** is presented in Fig. 1c. Each of the Zn(II) centre in the diacetato bridged dinuclear Zn(II) complex is five coordinated. According to τ value calculation[14] (τ = 0.372) the geometry around each Zn(II) centre is assumed to have distorted square pyramidal. From bond angle bond distance data, the pyridine nitrogen (N(4)), imine nitrogen (N(3)), thiolsulphur (S(1)) and one oxygen atom (O1) forms the base of the square pyramid whereas another oxygen atom of the acetate bridge (O(2^{i})) forms the apex. The difference between the maximum and minimum bond distances in the plane is 0.3862 Å. The larger bond distance (1.73 Å) here is suggestive of the thiolate form of the C-S bond of **L**[13].

Solution structures of 1 and 2

Solution structures of **1** and **2** were determined using EPR and NMR measurements. EPR spectrum of **1** (paramagnetic) in DMF and NMR spectrum of **2** (diamagnetic) in $CDCl_3$ were determined.

EPR study of 1

The anisotropic (axial) X-band EPR spectrum of **1** in DMF solution at room temperature is given in Supplementary Data, Fig. S2. The spectrum is found to have superhyperfine splitting which results from the coupling of the nucleus of coordinating N with the Cu(II)[15]. This predicts that the solid-state structure was retained in solution. The $g_{\perp}$ value was calculated as 2.02983 (Supplementary Data, Calculation I).

NMR analysis of 2

In ^{1}H NMR analysis of **2** (Supplementary Data, Fig. S3), the methyl protons attached to the carbon of the imine bond appear as singlet at 2.53 ppm, against the value of 2.35 ppm (Supplementary Data, Fig. S1) for free ligand. This is expected as the said protons are deshielded due to coordination of imine-N to the metal centre. The four aromatic protons attached to the pyridine moiety appear at 7.64–8.79 ppm as

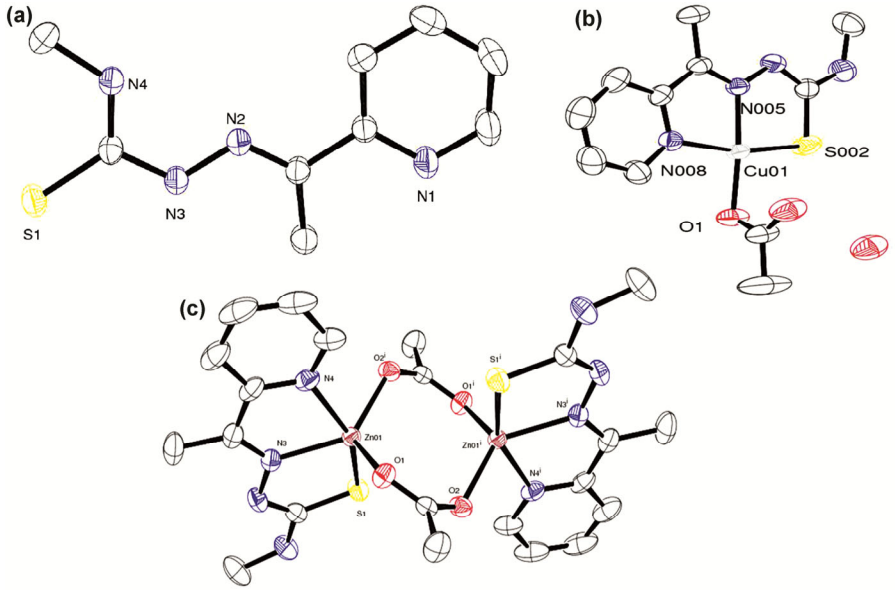

Fig. 1 — ORTEP plot of (a) ligand **L** and (b) complex **1** with 30% ellipsoid probability, and (c) complex **2** with 40% ellipsoid probability

multiplet. This on comparison to the value in the case of free ligand indicates the coordination of the pyridine nitrogen to the metal centre leading to deshielding effect resulting in appearance of the signals downfield. Signal at 1.98 ppm (singlet) appears because of the six methyl protons of the bridging acetate. Another singlet at 3.10 ppm is due to the terminal methyl protons attached to the secondary amine group in the ligand framework.

Anticancer activity

The anticancer activities of all three compounds were tested and compounds **L** and **2** were found to be equally toxic to both normal and cancer cell lines, hence these compounds were not further used for anticancer study. Whereas IC_{50} value of **1** in cancer cell line and normal cell line were 250 ng/mL (0.72 μM, in Supplementary Data, Calculation-II) and 500 ng/mL (1.44 μM, in Supplementary Data, Calculation-II and Fig. S4), respectively. The cell viability of normal cells was 93% up to 50 ng/mL of **1** while cell viability of cancer cells was 59%. In order to study molecular mechanism behind cell death, ROS levels were analysed using the molecular probe 2′,7′-dichlorofluorescein diacetate (DCFH-DA) (Fig. 2). The green fluorescence indicates the presence of ROS. DCFH-DA is the probe used for estimating the intracellular oxidative stress. The probe is cell permeable and on cellular uptake the probe is deacetylated by the intracellular esterase to a nonfluorescent DCFH carboxylate anion which in presence of ROS is oxidized to 2′,7′-dichlorofluorescein (DCF). DCF exhibits fluorescence which can be

Table 2 — Bond angle and distance parameters of compounds

Bond angles (°)			
L			
N(1)-C(5)-C(6)	115.59(14)	N(3)-C(8)-S(1)	119.30(12)
C(6)-N(2)-N(3)	118.13(13)	N(3)-C(8)-N(4)	116.79(14)
N(2)-N(3)-C(8)	118.53(13)	N(4)-C(8)-S(1)	123.91(12)
1			
N(005)-Cu(01)-O(1)	175.36(6)	N(005)-Cu(01)-S(002)	85.04(4)
N(005)-Cu(01)-N(008)	80.92(6)	O(1)-Cu(01)-S(002)	96.82(5)
O(1)-Cu(01)-N(008)	96.96(6)	N(008)-Cu(01)-S(002)	165.63(4)
2			
O(1)-Zn(01)-S(1)	111.32(5)	$O(2^i)$-Zn(01)-N(3)	130.44(6)
O(1)-Zn(01)-$O(2^i)$	117.11(6)	$O(2^i)$-Zn(01)-N(4)	88.34(6)
O(1)-Zn(01)-N(3)	109.32(6)	N(3)-Zn(01)-S(1)	80.70(5)
O(1)-Zn(01)-N(4)	89.23(6)	N(3)-Zn(01)-N(4)	75.53(7)
$O(2^i)$-Zn(01)-S(1)	97.24(5)	N(4)-Zn(01)-S(1)	152.76(5)
$O(1^i)$-Zn(01^i)-S(1^i)	111.32(5)	O(2)- Zn(01^i)-N(3^i)	130.44(6)
$O(1^i)$- Zn(01^i)-O(2)	117.11(6)	O(2)- Zn(01^i)-N(4^i)	88.34(6)
$O(1^i)$- Zn(01^i)-N(3^i)	109.32(6)	N(3^i)- Zn(01^i)-S(1^i)	80.70(5)
$O(1^i)$- Zn(01^i)-N(4^i)	89.23(6)	N(3^i)- Zn(01^i)-N(4^i)	75.53(7)
O(2)- Zn(01^i)-S(1^i)	97.24(5)	N(4^i)- Zn(01^i)-S(1^i)	152.76(5)
Bond distances (Å)			
L			
C(6)-N(2)	1.282(2)	N(4)-C(8)	1.320(2)
N(2)-N(3)	1.3762(18)	C(8)-S(1)	1.6874(15)
N(3)-C(8)	1.3640(19)		
1			
Cu(01)- N(005)	1.9529(14)	Cu(01)- N(008)	2.0087(15)
Cu(01)- O(1)	1.9536(12)	Cu(01)- S(002)	2.2308(5)
S(002)-C(00C)	1.7503(19)		
2			
Zn(01)-S(1)	2.3679(6)	Zn(01)-O(2)	2.0135(14)
Zn(01)-O(1)	1.9817(14)	Zn(01)-N(3)	2.1076(17)
Zn(01)-N(4)	2.1408(17)	Zn(01^i)-S(1^i)	2.3679(6)
Zn(01^i)-O(2^i)	2.0135(14)	Zn(01^i)-O(1^i)	1.9817(14)
Zn(01^i)-N(3^i)	2.1076(17)	Zn(01^i)-N(4^i)	2.1408(17)
S(1)-C(2)	1.730(2)		

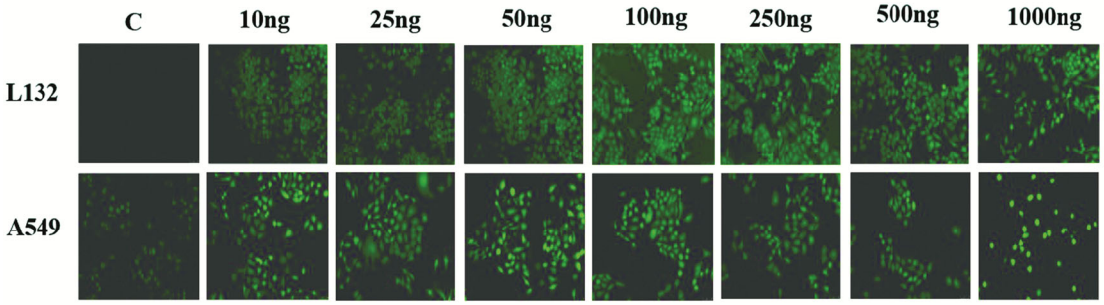

Fig. 2 — ROS generation by complex **1** with its increasing concentration

measured using a fluorescence microscope with excitation and emission at 485 nm and 535 nm, respectively. The ROS generation of control (C) cells was significantly low whereas, upon treatment with **1**, a significant ROS generation was observed in cancer cells. The ROS generation in normal cell was comparatively lower than that of the cancer cell. The increase in the ROS results in oxidant challenge to the cell which results in activation of cell death pathway finally resulting in the death of the cell. The result indicate that the treatment of **1** results in activation of high ROS challenge in cancer cells indicating that at the concentration used it specifically kills the cancer cell sparing the normal cells. The results thus indicated that the cell death mediated by **1** was observed to be through ROS generation. Mn(II) complex of the same ligand and its cytotoxicity against cancerous cells were previously reported[13]. The anticancer activity of this Cu(II) complex of **L** is a new addition to the existing literature in this field. Copper is one of the essential elements in various physiological processes and binds with DNA resulting in its damage and cell apoptosis through ROS formation[17]. The may be the reason for the better activity of **1** than **2** towards cancer cell lines.

Conclusions

Thiosemicarbazone ligand and its Cu(II) and Zn(II) complexes were synthesized and crystallographically characterized. Among these three, the Cu complex has shown promising anticancer activity against human lung cancer cell line. It is interesting to note that the IC_{50} value of this complex is almost 10^3 times lower than standard cisplatin. IC_{50} values of cisplatin against A549 cell line is 6 μM[16], whereas the value for Cu complex is less than 1 μM (0.72 μM). The molecular mechanism behind cell death in cancer cell lines using the concerned compound is found to be through the formation of reactive oxygen species.

Supplementary Data

Supplementary data associated with this article are available in the electronic form at http://nopr.niscair.res.in/jinfo/ijca/IJCA_60A(04)531-537_SupplData.pdf.

Acknowledgement

One of the authors (AC) is thankful to PURSE Phase II (Govt. of India) for his fellowship. Single crystal X-ray diffraction facility at USIC, Burdwan University, NMR at Visva Bharati, Santiniketan and EPR facility at SAIF, IIT Bombay are also gratefully acknowledged.

References

1 (a) Cai P, Xiong Y, Yao Y, Chen W & Dong X, *New J Chem,* 43 (2019) 14102; (b) Bisceglie F, Bacci C, Vismarra A, Barilli E, Pioli M, Orson N & Pelosi G, *J Inorg Biochem,* 203 (2020) Article ID 110888.

2 (a) Anjum R, Palanimuthu D, Kalinowski D S, Lewis W, Park K C, Kovacevic Z, Khan I U & Richardson D R, *Inorg Chem,* 58 (2019) 13709; (b) Sobiesiak M, Cieślak M, Królewska K, Kaźmierczak-Barańska J, Pasternak B & Budzisz E, *New J Chem,* 40 (2016) 9761.

3 Basuli F, Peng S M & Bhattacharya S, *Inorg Chem*, 39 (2000) 1120.

4 (a) Yuan C, Wang W, Wang J, Li X, Wu Y B, Li S, Lu L, Zhu M, Xing S & Fu X, *Chem Commun,* 56 (2020) 102; (b) Rébé C, Demontoux L, Pilot T & Ghiringhelli F, *Biomolecules*, 10 (2020) 13.

5 Dasgupta S, Karim S, Banerjee S, Saha M, Saha K D & Das D, *Dalton Trans*, 49 (2020) 1232.

6 Beraldo H & Gambino D, *Mini-Rev Med Chem,* 4 (2004) 31.

7 (a) Jain S K, Garg B S & Bhoon Y K, *Spectrochim Acta A,* 42 (1986) 959; (b) Hossain M E, Alam M N, Begum J, Ali M A, Nazimudhin M, Smith F E & Hynes R C, *Inorg Chim Acta,* 249 (1996) 207.

8 (a) Mal S K, Mitra M, Kaur G, Manikandamathavan V M, Kiran M S, Choudhury A R, Nair B U & Ghosh R, *RSC Adv*, 4 (2014) 61337; (b) Mal S K, Chattopadhyay T, Fathima A, Purohit C S, Kiran M S, Nair B U & Ghosh R, *Polyhedron,* 126 (2017) 23.

9 Hussein M & Guan T S, *Eur J Chem,* 6 (2015) 451.

10 Sheldrick G M, *Acta Cryst,* A71 (2015) 3.

11 Farrugia L J, *J Appl Cryst,* 45 (2012) 849.
12 Ghosh A K, Yadav H R, Duraipandian N, Choudhury A R, Kiran M S & Ghosh R, *Indian J Chem,* 56A (2017) 616.
13 Li M X, Chen C L, Zhang D, Niu J Y & Ji B S, *Eur J Med Chem,* 45 (2010) 3169.
14 Pal A, Biswas B, Mondal S K, Lin C H & Ghosh R, *Polyhedron,* 31 (2012) 671.
15 Prushan M J, Addison A W & Butcher R J, *Inorg Chim Acta*, 300-302 (2000) 992.
16 Swaminathan S, Haribabu J, Kalagatur N K, Konakanchi R, Balakrishnan N, Bhuvanesh N & Karvembu R, *ACS Omega,* 4 (2019) 6245.
17 Liu Y -H, Li A, Shao J, Song X-Q, Xie C-Z, Bao W-G & Xu J-Y, *Dalton Trans,* 45 (2016) 8036.